Comparison of morphological dating models for cumulative reverse fault scarps

S. Carretier,[1] F. Lucazeau, J.-F. Ritz, and H. Philip

Laboratoire de Géophysique Tectonique et Sédimentologie, UMR 5573, Université Montpellier II, Montpellier, France

Received 25 October 2001; revised 8 February 2002; accepted 13 February 2002; published XX Month 2002.

[1] Degradation morphology of scarps can be used to estimate the age of an episode of uplift: linear diffusion models for slope degradation provide analytical solutions relying on simplified geometry and kinematics. In this paper, we evaluate to what extent such models can be applied to date cumulative reverse fault scarps by comparing their predicted degradation coefficients with those of a more realistic numerical model. Two analytical models with increasing complexity have been considered; the CU and IU models represent the morphological evolution of a single vertical fault at a constant rate of uplift and that of a vertical fault shifting incrementally, respectively. Synthetic data are generated by a numerical model accounting for reverse faulting, linear diffusion, and gravity-controlled collapse. We show that for cumulative reverse faulting without folding, approximated models neglecting fault dip and gravitational collapse lead to valid estimates of the degradation coefficient in a lot of cases because gravitational collapse and reverse faulting are competitive geomorphic processes. We provide estimates of the shifts expected on the degradation coefficient according to neglected processes. *INDEX TERMS:* 1824 Hydrology: Geomorphology (1625); 7230 Seismology: Seismicity and seismotectonics; 1815 Hydrology: Erosion and sedimentation; 8010 Structural Geology: Fractures and faults; 8107 Tectonophysics: Continental neotectonics; *KEYWORDS:* morphological dating, reverse faulting, diffusion, earthquake

Citation: Carretier, S., F. Lucazeau, J.-F. Ritz, and H. Philip, Comparison of morphological dating models for cumulative reverse fault scarps, *J. Geophys. Res.*, *107*(0), XXXX, doi:10.1029/2000JB000028, 2002.

1. Introduction

[2] Estimation of the uplift rates in active areas, as well as the age of landscapes, can be inferred from the degradation morphology of escarpments [e.g., *Nash*, 1984; *Hanks and Schwartz*, 1987; *Avouac and Peltzer*, 1993; *Enzel et al.*, 1996; *Arrowsmith et al.*, 1998]. Leveling across scarps and inversion of topographic profiles with simple linear diffusion models can provide an estimate of the degradation coefficient $\tau = Kt$, the product of the mass diffusivity parameter K (m^2/yr) by the duration t (years) of an interseismic period following the offset of the topography [e.g., *Andrews and Hanks*, 1985]. If the mass diffusivity parameter can be calibrated, escarpments as old as 100 ka can be dated in arid regions, where erosion rate is low and landforms preserved [*Hanks*, 1999].

[3] When escarpments result from a single event, for instance one earthquake creating a fault scarp [e.g., *Nash*, 1984; *Hanks et al.*, 1984; *Hanks and Schwartz*, 1987; *Enzel et al.*, 1996] or a fluvial terrace scarp [e.g., *Hanks and Wallace*, 1985; *Avouac and Peltzer*, 1993; *Nivière et al.*, 1998; *Nivière and Marquis*, 2000], simple analytical solution of the diffusion equation with known initial conditions gives valuable estimates of Kt. The morphology of cumulative scarps, that recorded several events, may be used to estimate uplift rates on longer periods of time [e.g. *Avouac and Peltzer*, 1993; *Arrowsmith et al.*, 1998; *Mattson and Bruhn*, 2001]. However, geological conditions are more complicated and can involve variable dip of faults, several overlapping events, and migration of the surface uplift location. Therefore, geomorphological models of a higher level of complexity are supposed to be required to date such scarps, but their level of complexity has not been determined yet clearly for cumulative reverse fault scarps. *Hanks et al.* [1984] proposed an analytical solution of the diffusion equation based on the assumption that cumulative scarps morphology can be described by a constant uplift rate on a vertical fault. Greater number of geomorphic processes can be taken into account by numerical modeling [e.g., *Avouac and Peltzer*, 1993; *Arrowsmith et al.*, 1996; *Arrowsmith et al.*, 1998; *Mattson and Bruhn*, 2001], but the geological constraints to describe all the processes involved are usually not available. The main reason for this is that a trench at the location of a several meters high scarp profile is not always available. A trench is necessary to determine clearly the number of events, the location, and the shallow geometry of the successive faults. At most, some morphological evidences allow an estimate of the value of the vertical incremental offset, or/and to evaluate if all the scarp reactivations were located at the same place or not. For example, an asymmetrical scarp can result from variable location of the scarp reactivation at each event [e.g., *Avouac and Peltzer*, 1993; *Nivière and Marquis*, 2000].

[1] Now at Bureau de Recherches Géologiques et Minières, Orleans, France.

0148-0227/02/2000JB000028$09.00

Therefore, evaluating the limits of dating models and defining the conditions of their applicability to cumulative reverse fault scarps is of primary interest.

[4] To address this issue, we have developed a numerical model that can account for dipping faults, gravitational collapse, several successive uplifts events, horizontal offsets associated with faulting, and slope erosion. We generated synthetic scarp profiles for an extensive range of parameters (including incremental offset values, number of events, fault dips, distances between successive surface ruptures, and time lags between events), and we estimated the degradation coefficient from the synthetic profiles deduced from simpler models in which some of the processes are neglected. We restricted our study to reverse fault scarp and vertical fault scarps because the question addressed here has already been studied by *Avouac and Peltzer* [1993] for cumulative normal fault scarps. The simple models we tested are two analytical solutions of the diffusion equation. The first model is the analytical model proposed by *Hanks et al.* [1984], which accounts for continuous uplift along a vertical fault (continuous-uplift model). The second model is an analytical solution of the diffusion equation for a succession of offsets on vertical faults, that we derived in this analysis (incremental uplift model). We chose to evaluate the validity of such analytical models because the CU model has been used previously [*Hanks et al.*, 1984; *Mattson and Bruhn*, 2001], and because they only require parameters that can usually be estimated from scarp morphology. In the first part of this paper, we describe the different models, the numerical model behavior, and the method of inversion. Then, the result of inversions allow us to discuss in which extent the studied processes can be neglected.

2. Reverse Fault Scarp Evolution

[5] Scarps are submitted to slope erosion and may be incised locally by gullies. In portions of scarps preserved from incision, three main processes involved in the morphological evolution of cumulative reverse fault scarps can be distinguished [*McCalpin*, 1996] (Figure 1a): (1) offset of the surface with vertical and horizontal components and associated folding (instantaneous); (2) gravitational collapse of the hanging wall, leading to a gravity-controlled face at the slope of repose of the material (several months); (3) slope erosion by soil creep during interseismic periods between two uplift events. Folding can have variable amplitude and can affect significantly the morphology of a reverse fault scarp [e.g., *Philip and Meghraoui*, 1983; *Philip et al.*, 1992]. Additionally, reverse faulting can involve an unique planar fault cutting the surface, or a more complex geometry near the surface with secondary fractures, the splaying out of the fault, and variable location of the surface offset at each event [e.g., *Philip and Meghraoui*, 1983; *Meghraoui et al.*, 1988; *Swan*, 1988; *McCalpin*, 1996; *Yeats et al.*, 1997, p. 352]. Moreover, the complexity of the surface rupture can be variable along a fault scarp.

3. Numerical Model

[6] Morphologies of scarps in the real world result from a large variety of processes. Here we discuss conditions for which the numerical model is supposed to represent the real world.

[7] The numerical model is a one-dimensional (1-D) model based on the succession of the three first processes cited previously (points 1, 2, and 3) (Figure 1b), except the folding associated with reverse faulting which is not considered. Our study is thus restricted to cases for which folding has a minor effect on scarp morphology. We modeled planar faults (Figure 1). Their specified location at each event can be variable. The surface offset depends on the dip of fault and a specified vertical offset. Altitudes are translated from the fault location according to that offset (Figure 1). Soil creep erosion in portions of scarp preserved from gullies incision is classically modeled by a linear law relating the sediment mass flux per unit of width (q (m^2/yr)) to the local slope (S) [*Culling*, 1960] such as

$$q = K S, \tag{1}$$

where K (m^2/yr) is the mass diffusivity parameter. Combination of this erosion law and the conservation equation leads to a diffusion equation relying the erosion rate to the local curvature:

$$\frac{\partial h}{\partial t} = K \frac{\partial^2 h}{\partial x^2}, \tag{2}$$

where h is the elevation, t is the time, and x is the location. We use equation (2) to model the erosion during interseismic periods (Δt) during which the scarp acquires a degradation state characterized by a specified degradation coefficient $\Delta\tau = K\,\Delta t$ (m^2). The gravitational collapse occurring just after an event is modeled by increasing the mass diffusivity constant for slopes greater than a specified slope of repose *Sc*. Although the gravitational collapse is not a diffusive process, this numerical approach enables to form instantaneously a gravity-controlled face, that is consistent with field observations [e.g., *Wallace*, 1977; *Machette*, 1987]. The morphological evolution of a cumulative reverse fault scarp is modeled by repeating three successive phases: offset of the surface, gravitational collapse, and diffusion during interseismic periods. Diffusion equation is solved on a 300 m wide profile, so that the scarp evolution does not depend on the boundary conditions. Boundary conditions are constant elevation at the lower limit, and fixed elevation at the total offset value at the upper side. Our model is similar to that developed by *Avouac and Peltzer* [1993] for repeated normal faulting. The only difference apart from the reverse component of the faulting is that we solve the diffusion equation by explicit finite difference method rather than convoluting the topography with a gaussian erosion function. Both approaches lead to the same solution.

4. Numerical Model Behavior

[8] A parametrical study of this model was carried out varying the number of events, the offset increments, the dip of faults, the slope of repose, the interseismic duration, and the locations of the surface rupture. Different morphologies were obtained, that can be summed up in three overall cases (Figure 2). In the first case (Figure 2, case A), the morphology of the surface rupture due to localized reverse movement is being reset at each event by gravitational collapse. This occurred for large incremental offsets, faults cutting the

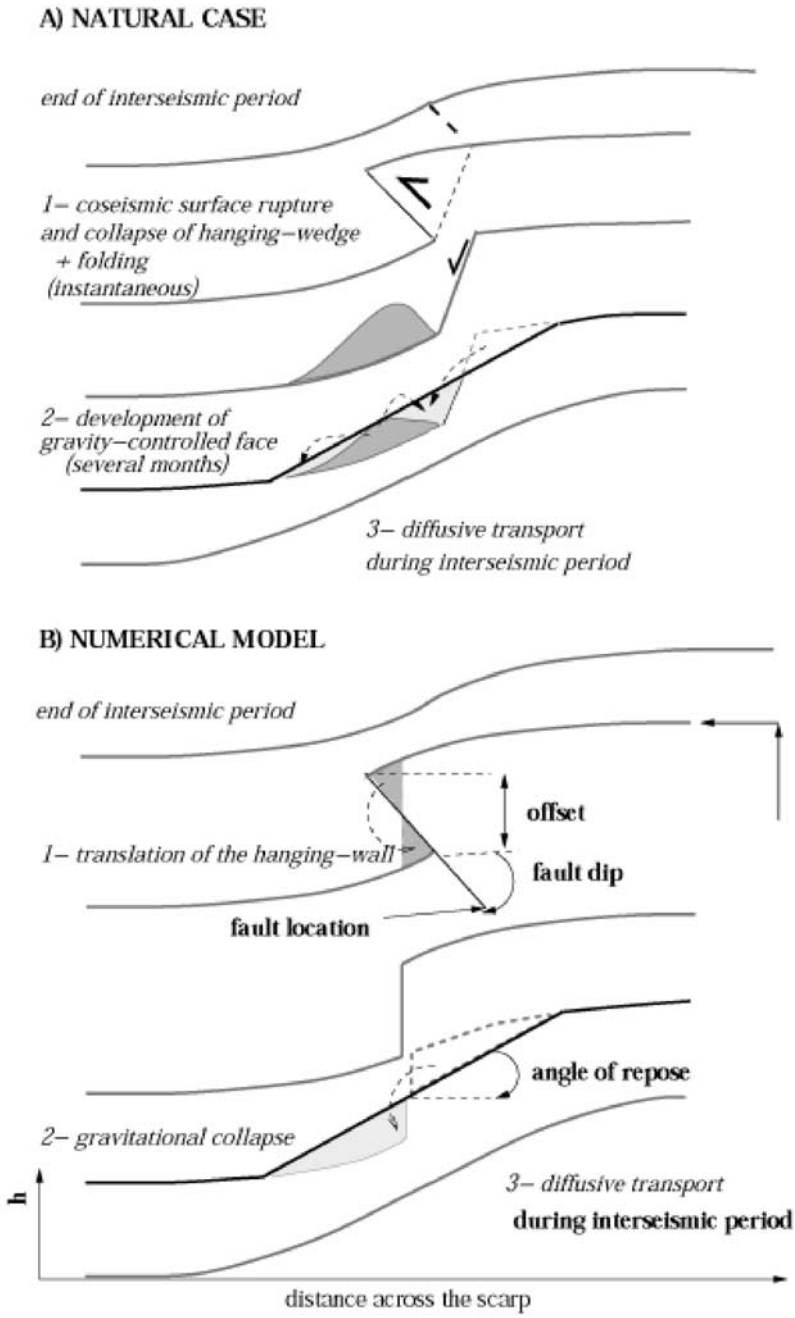

Figure 1. (a) Schematic evolution a reverse fault scarp degradation from the coseismic surface rupture, to the end of an interseismic period. (b) Schematic representation of the successive steps in the numerical model. The surface rupture occurs on a planar fault and the altitudes are translated from a specified fault location according to the vertical and horizontal offsets. Slopes greater than a specified slope of repose are reduced to this value. Then linear diffusion is applied during a specified interseismic duration.

surface roughly at the same place, and small interseismic durations. The resetting effect is enhanced for low dipping faults, because of scarp constriction due to the horizontal offset. Under those conditions, the morphological evolution of scarp is mainly controlled by gravitational collapse. In the second case (Figure 2, case B), successive faults are distant enough to preserve the morphology inherited from previous erosion periods, which leads to an asymmetrical scarp slope profile and individualized slope maxima. This morphology is favored for small offset increments compared to the distance between faults, and by short interseismic durations. For midrange values of these parameters, asymmetrical scarp profiles are obtained (Figure 2 case C). The slope distribution corresponds to embedded gaussian curves leading to a single slope maximum. This morphology is also favored by long interseismic periods. Cases A and C (Figure 2) are also obtained if secondary faults break the surface at each event, but remaining close to the main rupture. In such conditions, the gravitational collapse smooths the different surface offsets and the resulting

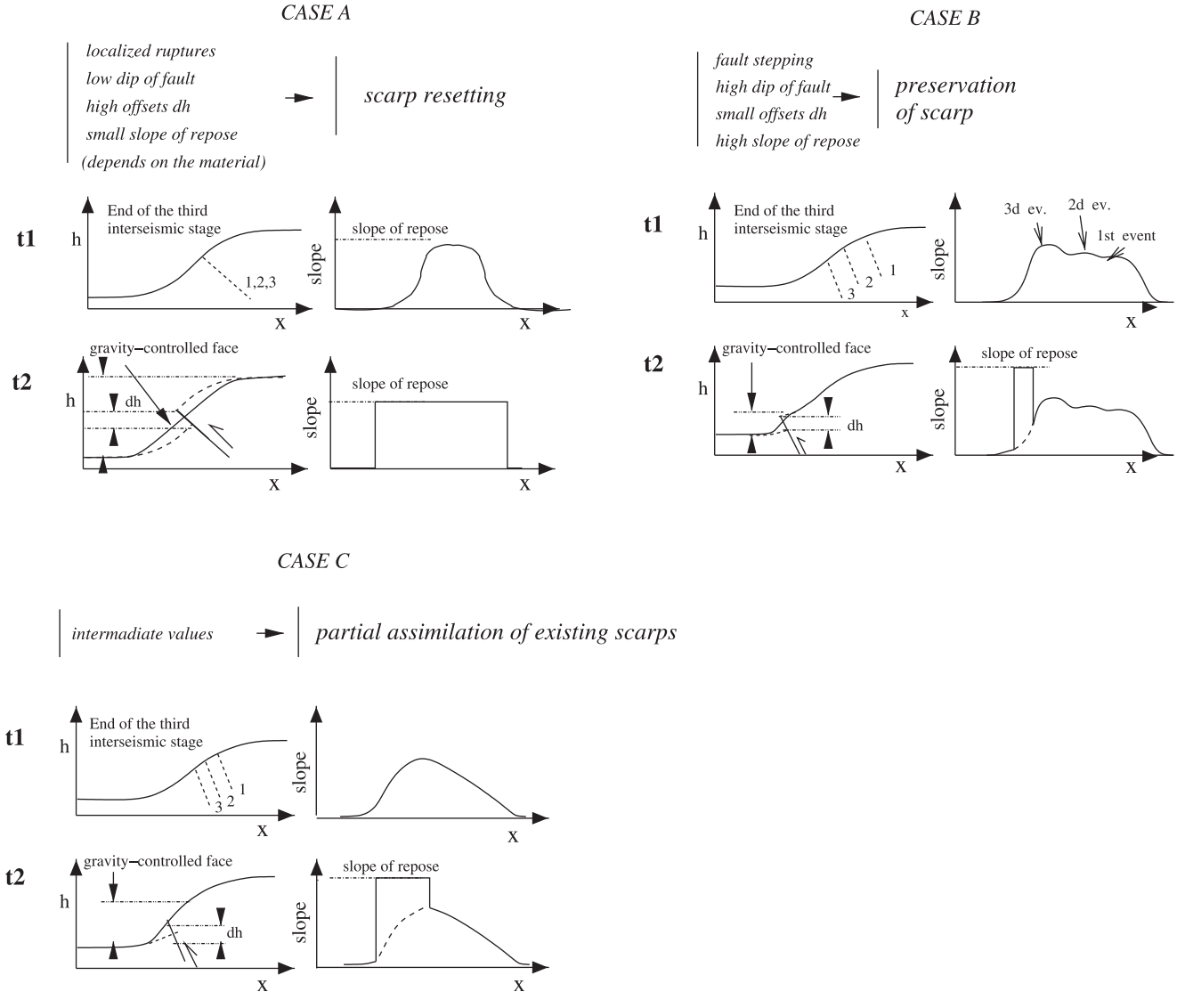

Figure 2. Schematic reverse fault scarp morphologies obtained with the numerical model. Case A corresponds to a single fault with a low dip and large offsets. These parameter imply a resetting of the scarp at each event because of the added effects of the scarp constriction and gravitational collapse. In case B, the fault steps at each event, preserving a wide portion of the scarp from gravitational collapse and allowing the morphology to keep the record of the successive surface offsets. In case C, The distance between faults is smaller and offsets values are intermediate between cases A and B. The record of variable fault location is only evidenced by the asymmetrical shape of the profiles. The size of the gravity-controlled face is intermediate between cases A and B, allowing the scarp to be preserved only at the top part.

morphology is equivalent to the morphology associated with a single main fault accounting for the total offset.

5. Analytical Models

5.1. Continuous Uplift Model (CU Model [*Hanks et al.*, 1984])

[9] *Hanks et al.* [1984] proposed an analytical solution of the diffusion equation (2) with an additional term for an uplift rate U:

$$\frac{\partial h}{\partial t} - K\frac{\partial^2 h}{\partial x^2} = \frac{U}{2}\,\mathrm{sign}(x), \tag{3}$$

where $\mathrm{sign}(x) = -1$ if $x < 0$ and $\mathrm{sign}(x) = +1$ if $x > 0$. Integrating (3) for initial conditions $h(x = 0,\ t = 0) = 0$ we find the analytical solution:

$$h_{\mathrm{cu}}(x,t) = \frac{U}{2}t\,\mathrm{erf}\left(\frac{x}{2\sqrt{\tau}}\right) + \frac{\frac{U}{2}x^2}{2K}\left[\mathrm{erf}\left(\frac{x}{2\sqrt{\tau}}\right) - \mathrm{sign}(x)\right] + \frac{\frac{U}{2}x}{K}\sqrt{\frac{\tau}{\pi}}\exp\left(\frac{-x^2}{4\tau}\right) + x\,b\ , \tag{4}$$

where b is the regional slope and $\tau = Kt$. This model assumes a vertical and fixed fault that separates the scarp in two symmetrical parts which move each other at constant rate U.

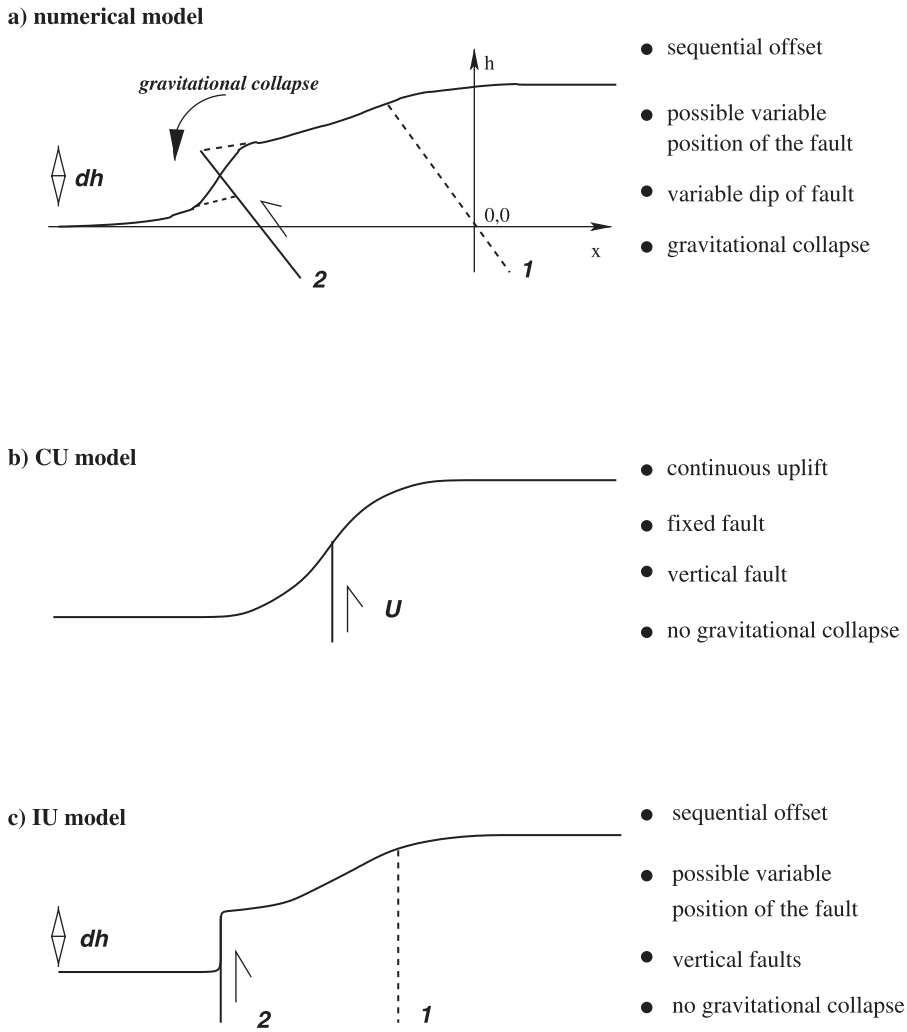

Figure 3. Assumptions of the different models. (a) Numerical model from which synthetic profiles are generated. (b) and (c) Analytical models based on simplified assumptions used to estimate the degradation coefficient.

[10] The basic assumptions of this model are (Figure 3): (1) the fault is planar and does not move with time, (2) the fault is vertical, (3) the uplift is continuous and constant over time, and (4) no gravitational collapse occurs. It can be noted that elevation profiles computed from this model are always symmetrical.

5.2. Incremental Uplift Model (IU Model)

[11] We introduce here another analytical solution of the diffusion equation which accounts for the sequential uplift and the possible variation of the surface rupture location. Thus this model accounts for an intermediate level of complexity between the continuous-uplift model and the numerical model. The basic assumptions of this model are (Figure 3) (1) the fault is planar, (2) the fault is vertical and can step at each event, (3) the uplift is sequential and corresponds to a succession of incremental offsets, and (4) no gravitational collapse occurs.

[12] According to these assumptions, the elevation $h_{IU}(x, t)$ were derived in the case of a number of events N and a planar initial surface (see Appendix A):

$$h_{\mathrm{IU}}\left(x,\tau=\sum_{i=1}^{N}\Delta\tau_i\right)=\sum_{i=1}^{N}\left(\frac{dh}{2}\right)i + \sum_{i=1}^{N}\left(\frac{dh}{2}\right)i\,\mathrm{erf}\left[\frac{x+\sum_{k=1}^{i}\Delta x_k}{2\sqrt{\sum_{k=i}^{N}\Delta\tau_k}}\right]+x\,b, \tag{5}$$

with $\Delta x_1 = 0$, where $(dh/2)_i$ is the half vertical offset associated to the event i, Δx_i the horizontal distance between two successive faults, and $\Delta\tau_i = K\Delta\tau_i$ the degradation coefficient between events i and $i + 1$. Assuming constant parameters ($(dh/2)_i = dh/2$, $\Delta x_i = \Delta\, x$, $\Delta\tau_i = \Delta\tau$), this solution becomes

$$h_{\mathrm{IU}}(x,\tau=N\Delta\tau)=N\,\frac{dh}{2}+\frac{dh}{2}\sum_{i=1}^{N}\mathrm{erf}\left[\frac{x+(N-i)\Delta x}{2\sqrt{i\,\Delta\tau}}\right]+x\,b \tag{6}$$

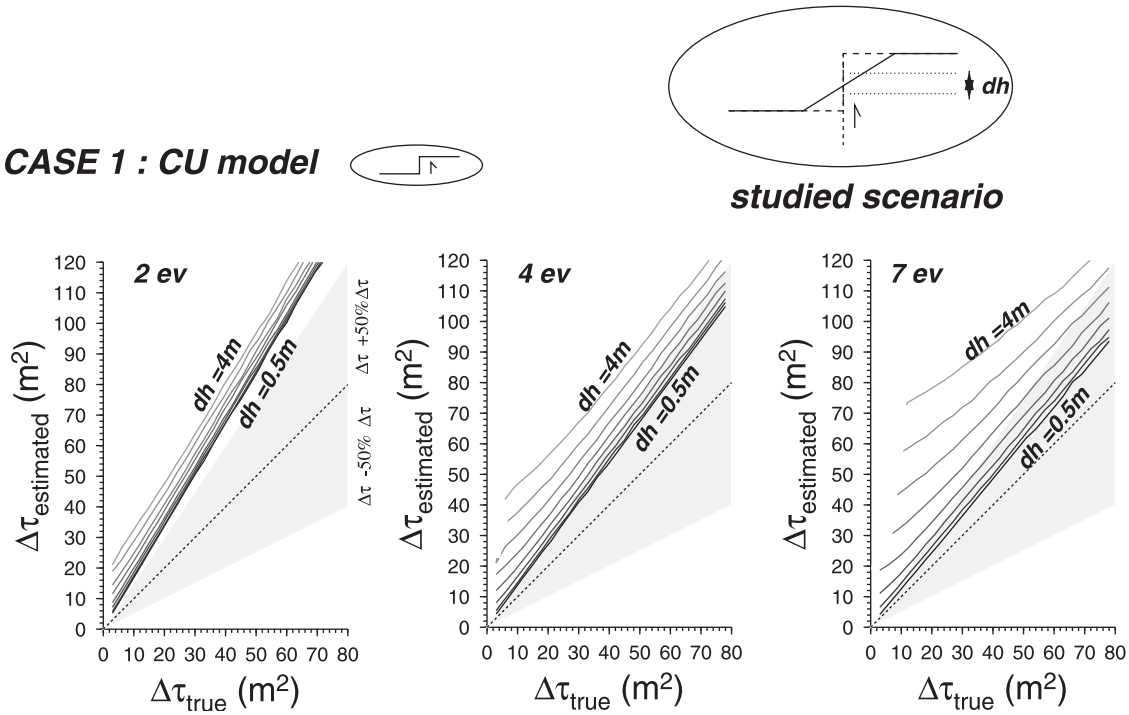

Figure 4. Results of inversions when neglecting repeated uplift and gravitational collapse with the CU model (case 1). The studied scenario is that for which synthetic profiles were generated with the numerical model. Results are given for 2, 4 and 7 events. Each graph shows $\Delta\tau_{estimated}$ versus $\Delta\tau_{true}$ curves for different offsets (*dh*) ranging between 0.5 m and 4 m by steps of 0.5 m. The dashed lines correspond to zero misfit between estimated and true values. The misfits between these values can be estimated graphically by the vertical shift between the dashed and the other curves. The limits of the shaded domain correspond to a ±50% relative error between estimated and true values.

Positive (negative) Δx values correspond to forward (backward) step of the fault at each event.

6. Inversion Method

[13] For simplicity, synthetic profiles are computed with constant values of the parameters at the end of the interseismic periods. Their elevation is sampled at constant intervals, and the first fault is located at the zero axis in the numerical model (Figure 3a), which defines the frame axis in which the inversion is carried out. Then, we use the analytical models (equations (4) and (6)) to calculate the degradation coefficient. In order to determine the best fitting value, a two-parameter search is performed in a least squares inversion:

1. The first parameter is the fault's location. Variable location of the surface rupture over time and the reverse component in the numerical model can produce asymmetrical synthetic profiles, constriction and shift of the scarp reactivation from the origin (Figure 3a). Because the analytical models do not account for all these behaviors, the search of the best fit between such a scarp profile and analytical solutions requires an adjustment of their fault locations. In the case of the IU model, the same number of events (faults) as in the numerical model is considered, while the CU model requires to adjust the location of a single fault.

2. The second parameter is the degradation coefficient. $\Delta\tau$ for the IU model and τ for the CU model.

[14] For each values of fault location and degradation coefficient, the root-mean-square (RMS) of the misfit between synthetic and modeled elevation profiles is calculated [e.g., *Avouac*, 1993; *Arrowsmith et al.*, 1998] as

$$\mathrm{RMS} = \sqrt{\frac{1}{n}\sum_{j=1}^{n}\left(h_{\mathrm{modeled}}(x_j) - h_{\mathrm{synthetic}}(x_j)\right)^2}, \qquad (7)$$

where n is the number of points x_j of the observed profile. For each value of fault location, the RMS versus $\Delta\tau$ (or τ in the case of the CU model) passed through a minimum value $\mathrm{RMS}_{\min}$ which corresponds to the best fitting value of $\Delta\tau$ (τ) [*Avouac*, 1993]. The preferred value corresponds to the minimum $\mathrm{RMS}_{\min}$ calculated over the whole range of tested faults locations. For each case, a sufficiently large range of parameters values was explored so that the optimum value of the degradation coefficient actually cor responds to the minimum of the RMS function. In practice, the adjustment of the faults locations implies that the distance between faults is different than the distance specified in the numerical model. For example, let us consider a synthetic scarp profile (taken as data) generated with two successive reverse faults at 0 m and −5 m in the ho-rizontal axis. The optimum distance between faults in the IU model will be smaller than 5 m to fit at best the shortening due to reverse faulting. On the other hand, the

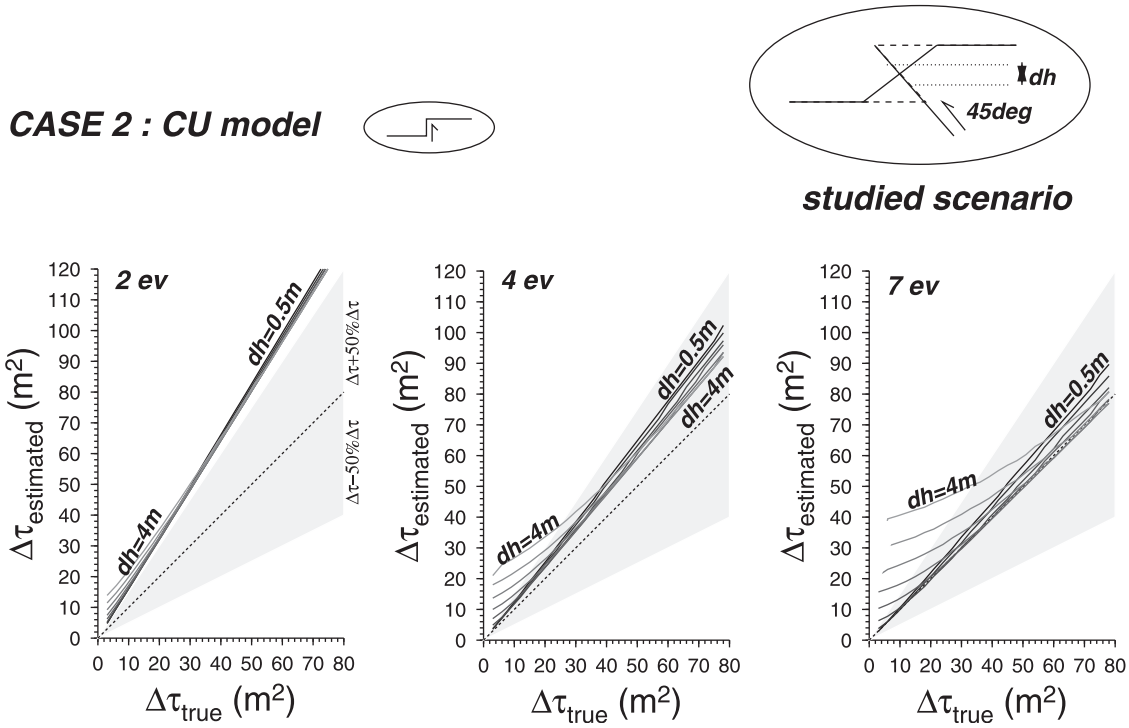

Figure 5. Results of inversions, when neglecting repeated uplift, gravitational collapse, and fault dip with the CU model (case 2). Same as Figure 4.

optimum unique vertical fault of the CU model will be located between 0 and −5 m.

7. Results

[15] The ability of analytical models to account for different tectonic settings can be evaluated by comparing estimated and true values of the degradation coefficient. The estimated value are the results of inversions, while the true values are set in the numerical model. These results are presented as a sets of neglected processes, for which the parameters could not be estimated in the field. Four different tectonic settings are studied, involving vertical or 45° dipping fault, and single or forward stepping faults. These choices correspond to extreme cases of reverse fault scarp morphologies (Figure 2). The slope of repose is set at tan30 in each case, that corresponds to the typical slope of repose of an unconsolidated material. The regional slope is set at b = 0 in each case.

7.1. Case 1: Neglecting Repeated Uplift and Gravitational Collapse With the CU Model

[16] Synthetic profiles are generated using a single vertical fault, repeated offsets, and gravitational collapse after each event. Figure 4 shows the $\Delta\tau$ values, defined as τ divided by the number of events, estimated from the CU model versus "true" $\Delta\tau$ values. The dashed line corresponds to $\Delta\tau_{estimated} = \Delta\tau_{true}$ and the shaded domains to $\Delta\tau$ estimates for which the relative error is lower than ±50% (%$(\Delta\tau_{estimated} - \Delta\tau_{true})/\Delta\tau_{true}$). Inverted $\Delta\tau$ values are plotted for different offset values, ranging from dh = 0.5 m to 4 m by steps of 0.5 m, and for 2, 4, and 7 events. The studied $\Delta\tau$ values lie between 2 and 80 m^2. For typical values of the mass diffusivity parameter ranging between 10^{-3} m^2/yr and 10^{-2} m^2/yr [*Hanks*, 1999], $\Delta\tau$ values correspond to durations between events ranging between 200 y and 80000 y, and slip rates ranging between 0.6×10^{-2} mm/yr to 2 cm/yr. In Figure 4, the shift between inverted and true $\Delta\tau$ values can be graphically determined from the vertical shift between the dashed line and the others. Results show that the degradation coefficient is overestimated in all cases. For small incremental offsets (dh < 2 m), this overestimate decreases with increasing number of events: small offsets increments and increasing number of events are a better approximate of a continuous uplift. For large offset increments on the other hand, misfit increases with the number of events because gravitational collapse affects a larger part of the scarp and is not taken into account by CU modelings.

7.2. Case 2: Neglecting Repeated Uplift, Gravitational Collapse, and Fault Dip With the CU Model

[17] Synthetic profiles are computed as previously but the fault is dipping at 45°. Figure 5 shows that the misfit between the true values and those estimated from the CU model decreases with increasing number of events for small values of dh. The misfit increases with offsets for small values of $\Delta\tau_{true}$, while it decreases for larger values. This behavior is different from the previous case involving vertical faults in the numerical model. The estimated $\Delta\tau$ are significantly better than in the previous case, especially for large offsets (compare Figures 4 and 5). For example, the CU model gives an accurate estimate of the degradation coefficient for the 7 events case, for dh = 2 m and $\Delta\tau_{true} >$ 20 m^2 (Figure 5). In the case of a vertical fault, the same set of parameters leads to a relative overestimate between 100% and 50%. This surprising result can be explained by the competitive morphological effects of the gravitational collapse and the shortening by reverse displacement. Reverse movement implies a constriction of the scarp, that appears

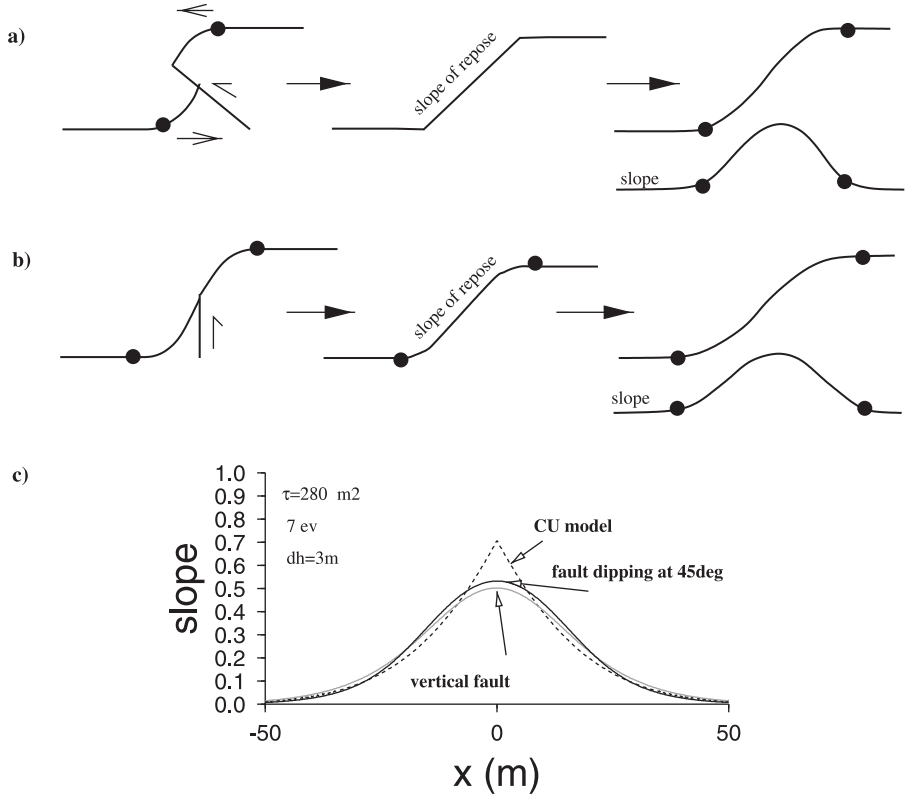

Figure 6. Why the CU model is a better approximate of a reverse fault scarp than a vertical fault scarp? (a) Reverse faulting implies a scarp constriction and favors the collapse of the scarp. (b) For a vertical fault, gravitational collapse affects a narrower portion of the scarp. The degraded scarp length (between the 2 points) is greater than in the previous case (Figure 6a) and the maximum slope is smaller. (c) Comparison of computed slope distributions for 2 scarps generated with the numerical model (vertical and 45° dipping fault) and one scarp generated with the CU model. The degradation coefficient is the same for the three profiles. Note that the profile generated with a reverse fault is narrower at the basis than for a vertical fault, while its maximum slope is greater. The CU model predicts also a narrower curve and a greater maximum slope than the model accounting for a vertical fault and gravitational collapse. Consequently, the CU model fits better the reverse fault case.

when comparing the slope profiles associated with a vertical fault and with a fault dipping at 45°: the second one is narrower than the first one at the basis (Figure 6). On the other hand, the gravitational collapse, enhanced by reverse displacement, favors the preservation of a large slope at the center of the profile after diffusion. Consequently, the maximum slope in the reverse fault case is greater than in the vertical fault case (Figure 6). *Arrowsmith et al.* [1996] noted that the CU model predicts a narrower scarp and a greater maximum slope than reality, because a large slope at the center of the profile is enhanced by the continuous uplift and the absence of slope threshold. However, these morphological misfits are reduced when a reverse movement is involved (Figure 6c). Thus this result suggests that a reverse fault scarp is better approximated by the CU model than a vertical fault scarp, for which the model was designed.

7.3. Case 3: Neglecting Repeated Uplift, Gravitational Collapse, and Variable Fault Location With the CU Model

[18] In this case (Figure 7), $\Delta\tau$ values are always overestimated. The overestimate does not depend significantly on the vertical offset value, but decreases with increasing number of events, especially for small $\Delta\tau$ values. For large offset increments, estimates are better than for a single vertical fault (compare Figures 4 and 7). Large offsets favor the scarp degradation by gravitational collapse, which affects a narrower portion of the scarp when the fault steps (Figure 2, case C). Gravitational collapse tends to make the synthetic profiles more symmetrical, while preserving a large portion of the scarp from resetting. This trade-off implies that the CU model is more valid if the rupture location actually moves. For small offset increments, estimated $\Delta\tau$ values are conversely not as good (compare Figures 4 and 7) because synthetic profiles are strongly asymmetrical, as a consequence of the fault migration and the minor effect of gravitational collapse in this case. Consequently, scarp profiles computed with CU model poorly fit the studied synthetic profiles.

7.4. Case 4: Neglecting Repeated Uplift, Gravitational Collapse, Variable Fault Location, and Fault Dip With the CU Model

[19] In this case (Figure 8), $\Delta\tau$ values are also systematically overestimated. The misfit decreases with increasing offset for high $\Delta\tau_{true}$ value. Moreover, while the misfits are

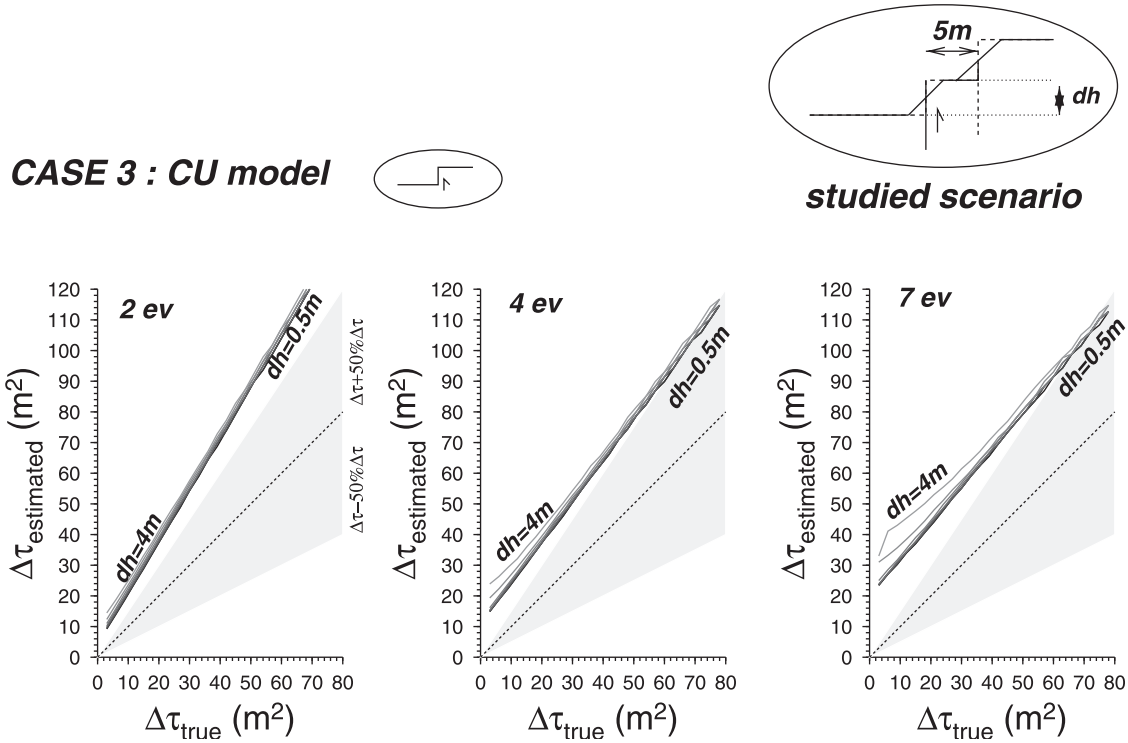

Figure 7. Results of inversions when neglecting repeated uplift, gravitational collapse and variable fault location with the CU model (case 3). Same as Figure 4.

similar to those of case 3 (compare Figures 7 and 8), results are significantly better for large offsets increments, and for increasing number of events. This is once again due to the scarp constriction related to reverse faulting. These results suggest that reverse faulting with variable fault location can be well approximated with the CU model, leading to relative errors on $\Delta\tau$ below 50% for most of the tested range of parameters.

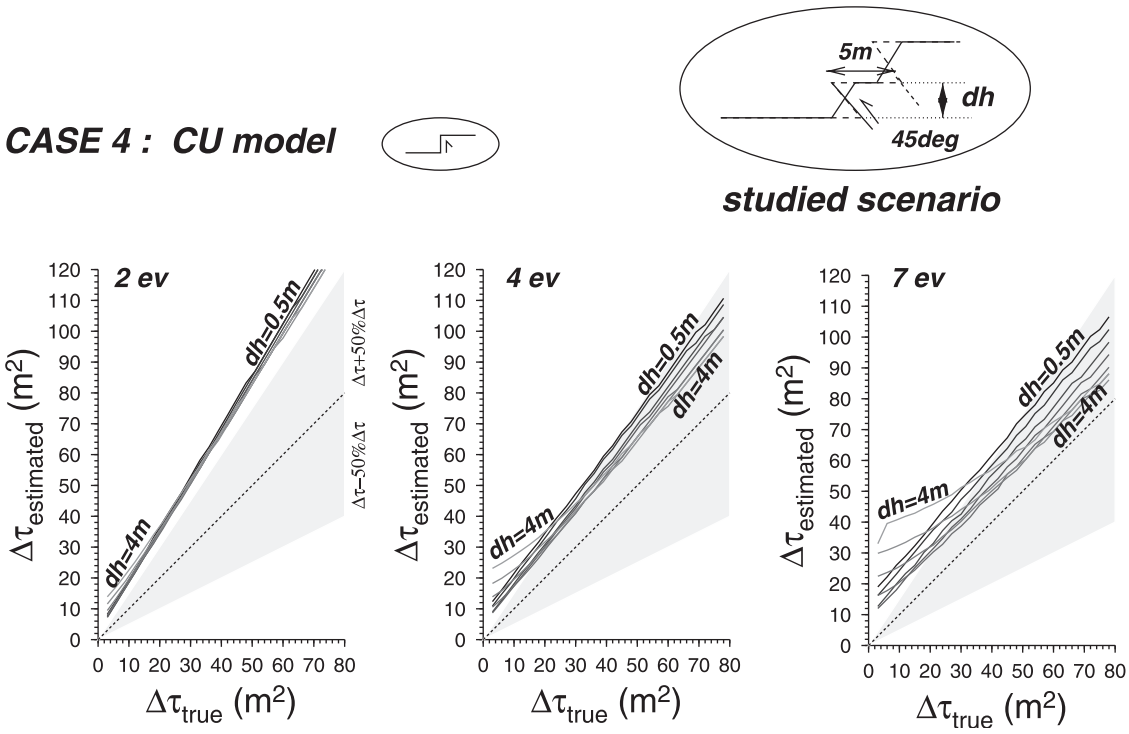

Figure 8. Results of inversion when neglecting repeated uplift, gravitational collapse, variable fault location and fault dip with the CU model (case 4). Same as Figure 4.

7.5. Case 5: Neglecting Gravitational Collapse With the IU Model

[20] Because the IU model accounts for fixed or variable fault locations, two scenarios are summed up in this section: Figure 9a shows the results for synthetic profiles computed with a single vertical fault, and Figure 9b shows the results when the fault location steps 5 m at each event.

[21] For the first case (Figure 9a), the inferred values of $\Delta\tau$ are overestimated, although this overestimate is very small. The overestimate increases with the value of *dh* and the number of events. This result is consistent with what we learned from studies of one event scarps. Comparison has been made with one event scarps morphologies corresponding either to an initial step-like geometry (analogue to IU model initial condition) or to an initial ramp-like geometry with a uniform slope [e.g., *Hanks*, 1999; *Nivière et al.*, 1998]. In the case of one event scarp and for $\tau/dh^2 \geq 1$, *Hanks* [1999] pointed out that "scarp degradation no longer cares about the initial condition, so long as the initial slope is $\geq$30°." In the case of cumulative scarp, large incremental offsets and increasing number of events favor the resetting by gravitational collapse. This leads to ramp-like geometry defined by a uniform slope (30° in our synthetic profiles) at each event (see Figure 2, case A). Such cumulative scarps behave as one event scarp for which a similar criterion can be applied ($\Delta\tau$/number of events $dh^2 \geq 1$). For example, the inverted $\Delta\tau$ is very closed to the true value for $\Delta\tau = 70$ m^2, 4 events and $dh = 4$ m. For these values, the criterion is $70/(4 \times 4^2) = 1.1 > 1$ (Figure 9a).

[22] When the fault location steps at each event (Figure 9b), results are significantly better. The difference between true and inverted values of $\Delta\tau$ is only significant for incremental offsets dh > 3 m. Although the step of scarp reactivation tends to preserve the scarp morphology from gravitational collapse (Figure 2, case B), this process becomes an important controlling factor for large offsets ($dh > 3$ m). These results suggest that neglecting gravitational collapse when modeling vertical fault scarps is valuable since rupture position varies and offset increments are lower than 3 m.

7.6. Case 6: Neglecting Gravitational Collapse and Fault Dip (IU Model)

[23] Figure 10a shows the $\Delta\tau$ values inverted by IU modeling when a single fault dipping at 45° is used for the numerical model. Unlike the vertical faulting case, $\Delta\tau$ can be underestimated. For example, the true value is 50 m^2 for 7 events and $dh = 4$ m, while the corresponding inverted value is 42 m^2 (Figure 10b). For small $\Delta\tau_{true}$ values and large offset increments, inverted values are greater than true one, because gravitational collapse becomes the main controlling process of scarp degradation (Figure 2, case A). Such synthetic profiles evolve from a ramp-like geometry acquired at each event by collapse. The positive misfits between inverted and true values is due to the discrepancy between such initial conditions and the step-like initial conditions of the IU model. They vanish and become negative when $\Delta\tau_{true}$ increase, because of the scarp constriction. This effect dominates when the degradation coefficient increases. Consequently, a scarp evolving with a reverse fault and long interseismic durations displays a lower apparent degradation state (coefficient) than a scarp evolving with a vertical fault.

[24] Repeating the last experiments but imposing a reverse fault stepping 5 m at each event provides results shown in Figure 10b. The misfits follow the same behavior as for the single fault models (Figures 10a and 10b). However, estimates are better because the variable location of the rupture preserves the scarp from gravitational collapse.

[25] In conclusion, reverse component and gravitational collapse interact to give either a less degraded or a more degraded apparent state to scarps. Neglecting these two processes implies an overestimate of $\Delta\tau$ for large offset increments and small interseismic durations, and an underestimate for long interseismic periods.

8. Discussion

8.1. Representativity of the Tested Tectonic Settings

[26] Although a wide range of parameters values have been investigated, the tested tectonic scenarios (vertical or dipping fault, single fault, or forward stepping faults) do not represent an exhaustive range of possible cases. Moreover, some of the tested cases may be strictly theoretical, with a poor fitting with reality. On the other hand, they may represent extreme cases of real scarp morphologies, as suggested by our parametrical study of the numerical model behavior (Figure 2). Our results may consequently be enlarged to other tectonic scenarios, that have the same effect in terms of scarp morphology. For example, secondary fractures associated with a main fault do not appear in the scarp morphology if gravitational collapse is efficient enough. It should also be noted that the forward stepping of a vertical fault may also represent the successive reactivations of a terrace riser by pulses of lateral incision of a river [e.g., *Nivière and Marquis*, 2000]. The folding associated with reverse faulting has not been taken into account in our study. Generally, folding leads to an overestimate of the degradation coefficient, because it gives an apparently more degraded morphology than the reality. Therefore, this geomorphic factor should affect the validity of a simple model applied to real case. Consequently, our results should not be extended to scarps strongly controlled by folding.

8.2. What Can Be Neglected?

[27] The objective of this study was to identify the conditions for which some processes involved in cumulative reverse fault scarp evolution could be neglected, with an "acceptable" error in the degradation coefficient determination. Formally, our results suggest that no process can be neglected, because estimates are always shifted from the true values. In some cases, the shift can be small. For example, neglecting gravitational collapse in the case of a near vertical fault provides an estimate of the degradation coefficient within +5% of relative error ($\%(\Delta\tau_{estimated} - \Delta\tau_{true})/\Delta\tau_{true}$), if $dh < 2$ m and $\Delta\tau > 20$ m^2 (this error can be estimated from Figure 9a and concerns the IU model). This value reaches 50% with the CU model neglecting repeated offsets and gravitational collapse associated with a near vertical fault (see Figure 4). A 50% relative error of the degradation coefficient leads to a −33% relative error of the mean uplift rate U defined as $\%(U_{estimated} - U_{true})/U_{true}$, where U = total offset/total time. For example, if we estimate a degradation coefficient within 50% relative error, and if the true slip rate is 1 mm/yr, we will estimate an uplift rate at 0.75

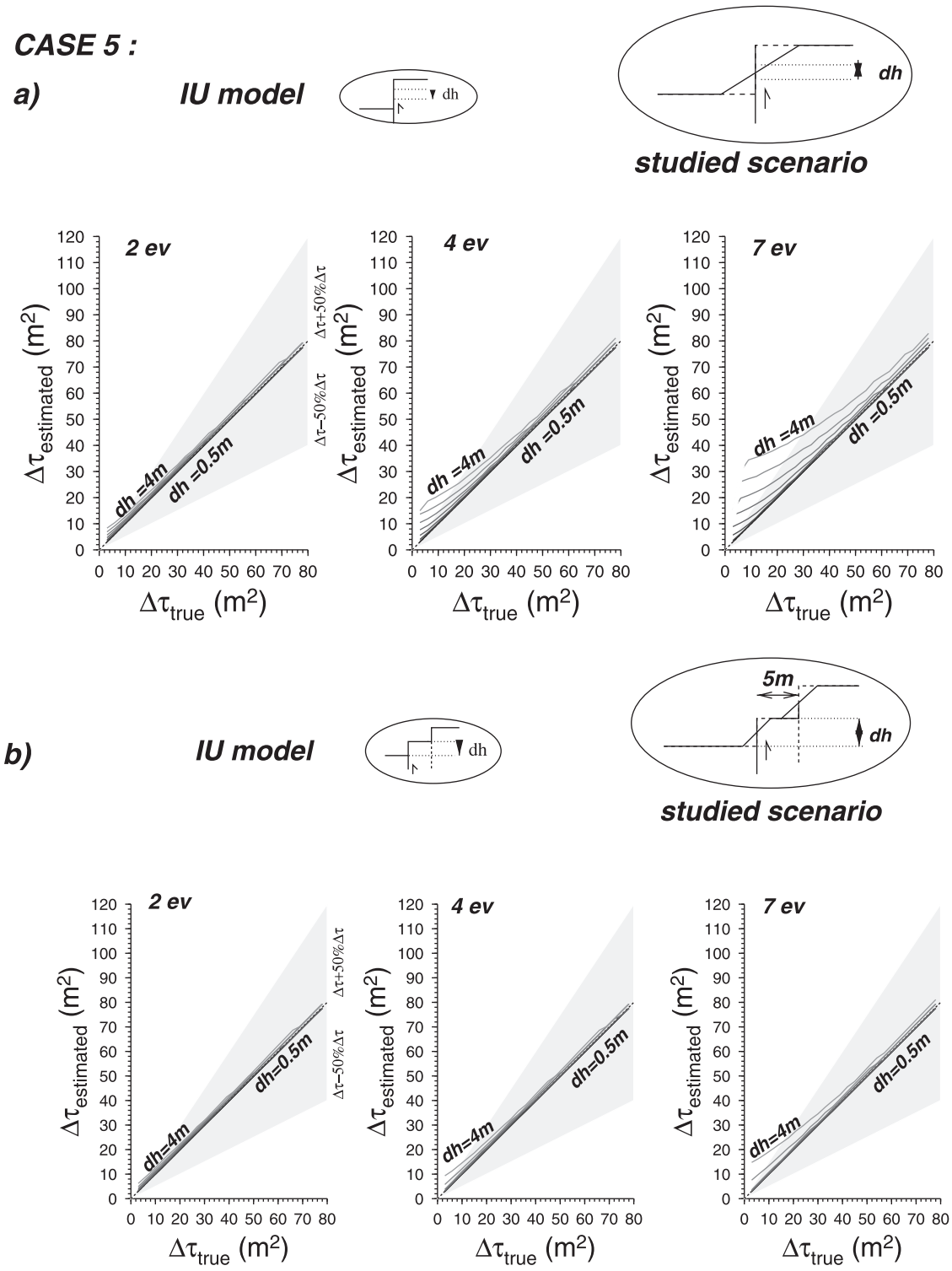

Figure 9. Results of inversions, when neglecting gravitational collapse with the IU model (case 5). (a) Studied synthetic profiles correspond to a succession of offsets on a vertical fault with gravitational collapse. (b) Same as Figure 9a but the fault steps 5 m at each event. Same as Figure 4.

mm/yr. In most cases, uncertainties on the dating techniques (e.g., cosmonucleides) are such, compared to the implications on fault behavior and seismic hazard, that the knowledge of the order of magnitude could be quite sufficient: main questions that arise in active tectonics are to know if fault slip is 1 mm/yr or 10 mm/yr, rather than if it is 0.75 mm/yr or 1 mm/yr. Therefore, if we accept a relative error lower than ±50% for the degradation coefficient, the parameters range for which this criterion is valid can be determined from our results for each set of neglected process. Figure 11 displays

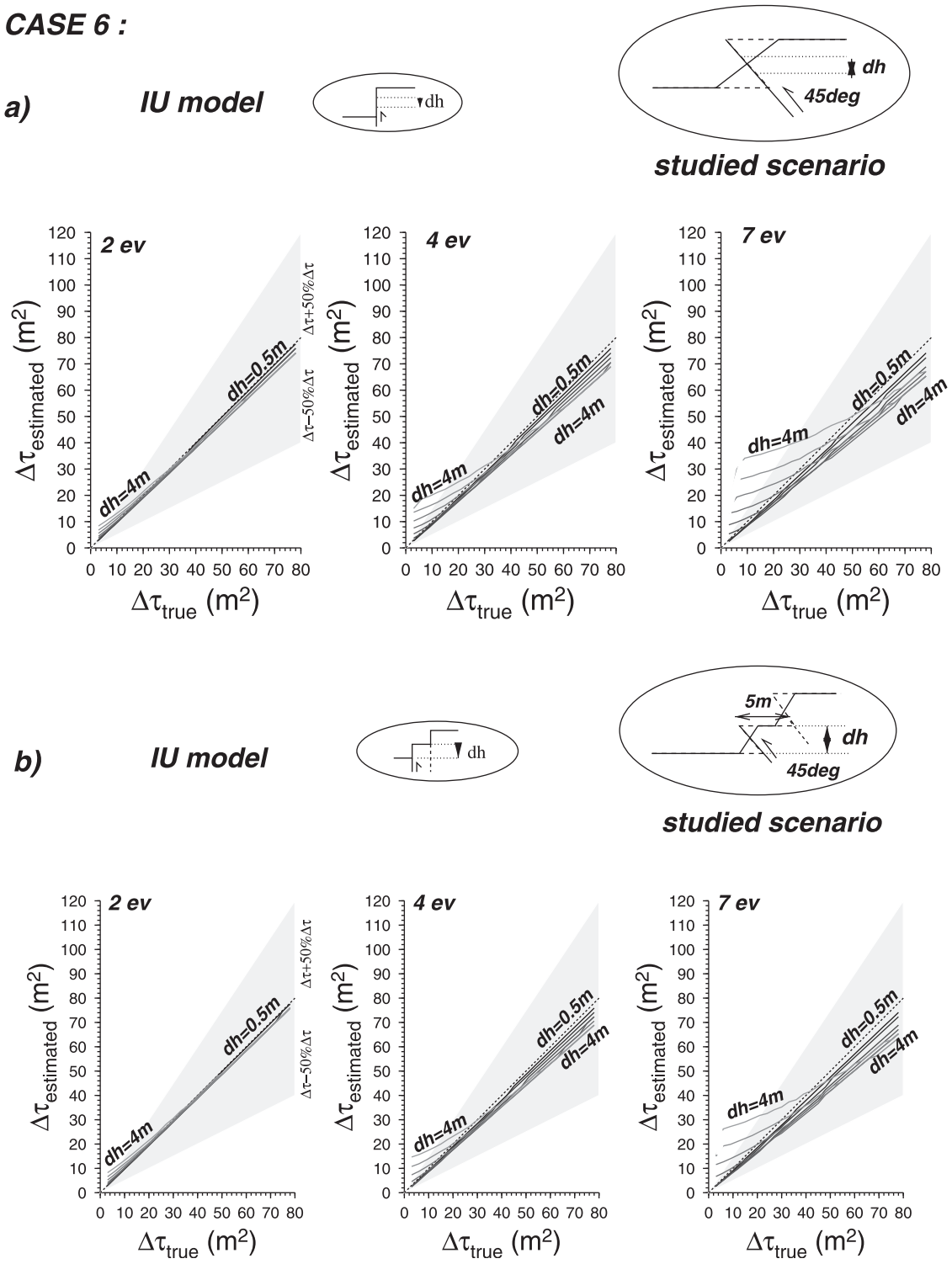

Figure 10. Results of inversions when neglecting gravitational collapse and the fault dip with the IU model (case 6). (a) Studied synthetic profiles correspond to a succession of offsets on a 45° dipping fault with gravitational collapse. (b) Same as Figure 10a but the fault steps 5 m at each event. Same as Figure 4.

the $\Delta\tau$ versus *dh* ranges for which scarp modelings with the CU model (Figure 11a) and the IU model (Figure 11b) give estimate of the degradation coefficient within a relative error lower than ±50%, both for fixed and stepping fault cases. In most of the cases, this error is positive, except for IU model in the case of fault dipping at 45° and large $\Delta\tau$ values (see Figure 10). Figure 11 illustrates the most striking results we obtained: the more simple model (CU model) gives better estimates of the degradation for dipping faults than for vertical faults, and remains valid for some stepping fault cases, although CU model is based on a one vertical fault assumption. This suggests that different faulting combined

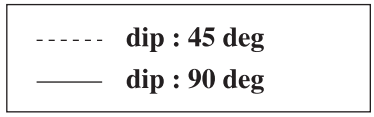

a) CU model (neglecting repeated offsets, grav. coll., fault dip, var. fault loc.)

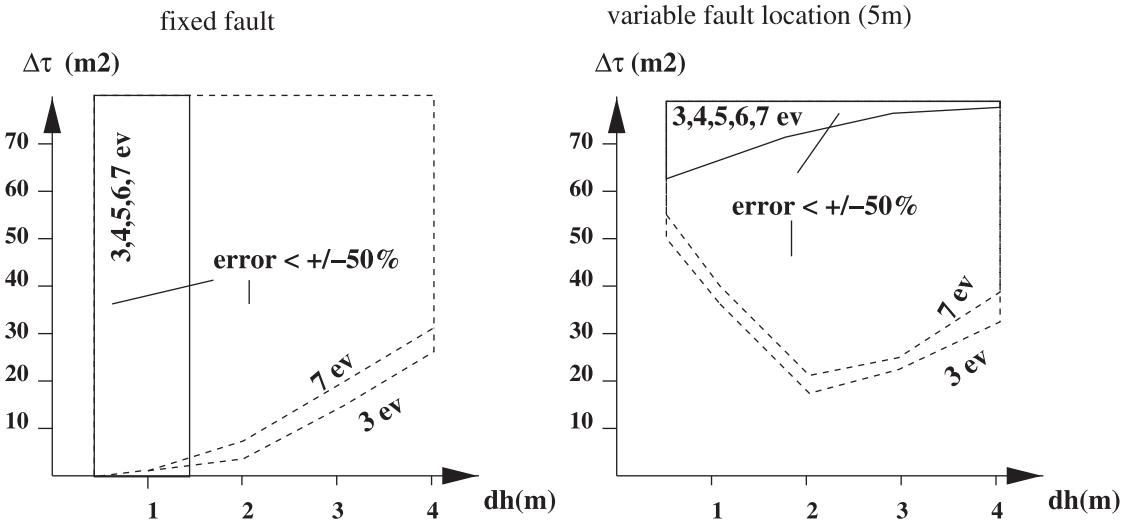

b) IU model (neglecting grav. coll. and fault dip)

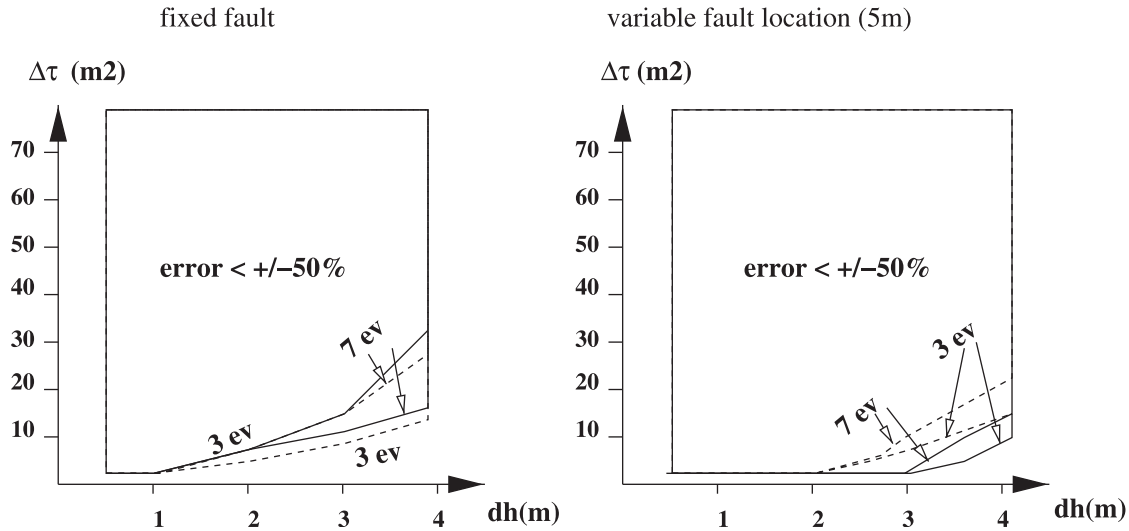

Figure 11. $\Delta\tau$ versus offsets (*dh*) domains, for which the relative misfits between estimated and true $\Delta\tau$ values are lower than ±50%. (a) CU model. (b) IU model.

with different degradation processes may produce similar scarp morphologies. However, this lack of uniqueness in scarp modeling can be used positively. It allows us to neglect some processes for which the parameters are difficult to estimate with accuracy on the field (for instance the fault dip or the incremental offset values). For example, let us consider a scarp for which there are some morphological evidences that the reverse fault has a dip lower than 90° and that the surface ruptures occurred roughly at the same place and that each incremental offset lies between 2 m and 3 m, for respectively 6 and 4 events to achieve a cumulative offset of 12 m. The results we obtained suggest that the degradation coefficient inferred from CU modeling will be overestimated with a maximum at 50% relative error (Figures 5 and 11a), and therefore the CU model will provide an acceptable estimate. Similarly, a relative error can be estimated for the IU model. Generally, our results can provide estimates of the error expected when unknown parameters are neglected. However, the errors given in this study are only valid for a whole profile inversion. The shifts could be greater if the

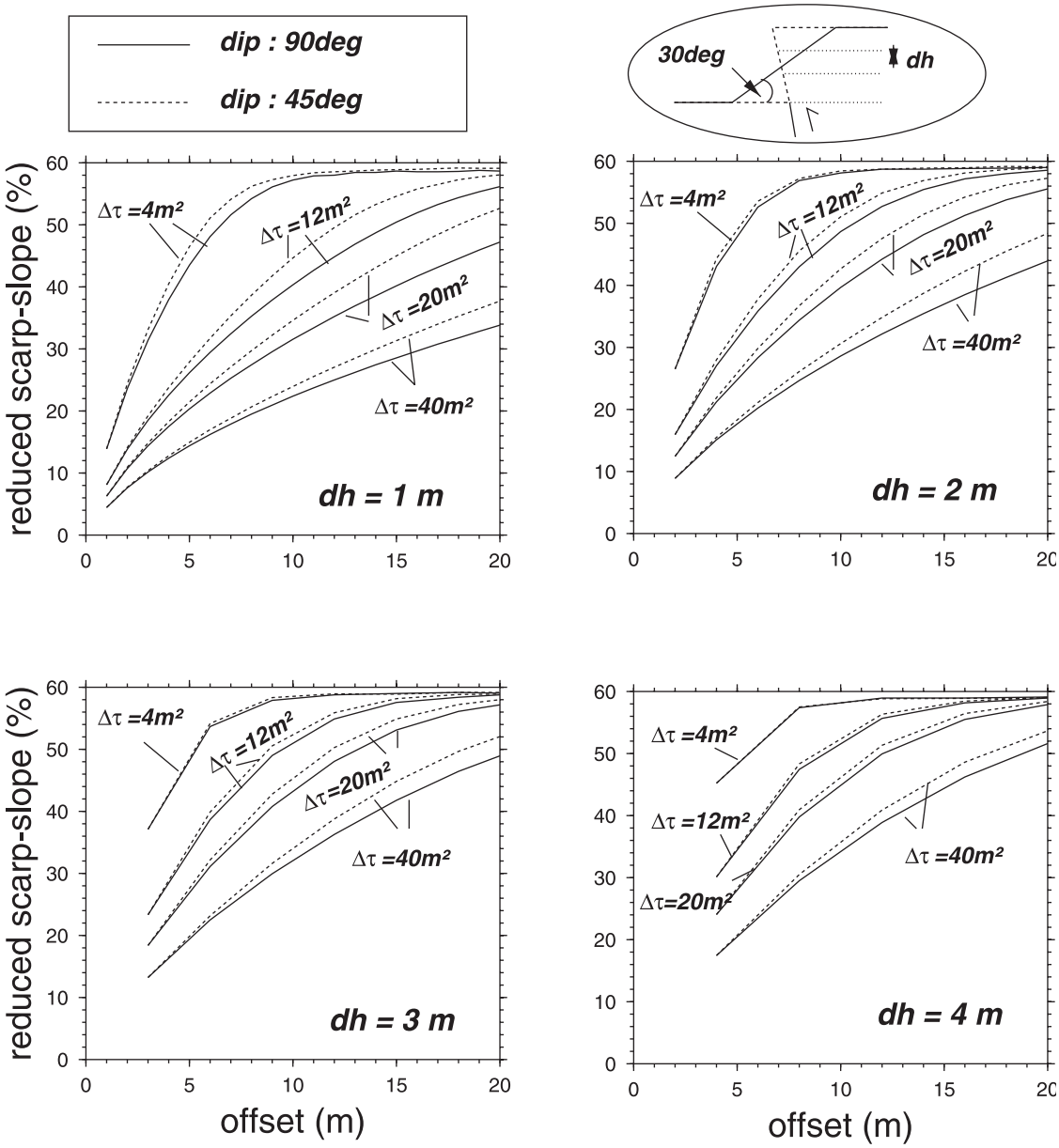

Figure 12. Comparison of scarp slope versus cumulative offset obtained with the numerical model for a single fault with various set of parameters *dh*, $\Delta\tau$, and fault dip. For a typical value of the mass diffusivity parameter K at 310^{-3} m^2/yr in arid regions [e.g., *Avouac and Peltzer*, 1993], $\Delta\tau$ values of 4, 12, 20, and 40 m^2 correspond to interseismic durations of 1300, 4000, 6600, and 13,300 years, respectively. The corresponding slip rates for *dh* = 1, 2, 3, and 4 m range from 0.07 to 3 mm/yr. Note that for a typical value of the mass diffusivity parameter K at 310^{-3} m^2/yr, the reduced scarp slope will saturates very quickly for interseismic durations lower than 1300 years, that can occur at a plate boundary as well as in some other active regions like central Asia [e.g., *Avouac*, 1991].

degradation coefficients have been estimated from the maximum slope only (in particular for the CU model [*Arrowsmith et al.*, 1996]).

8.3. Dating Strategy

[28] In previously published works, two dating strategies have been carried out to date scarps. On the one hand, scarp degradation modeling have been used to estimate a degradation coefficient of one event scarp or cumulative scarp from their whole morphology [e.g., *Hanks et al.*, 1984; *Avouac*, 1993; *Arrowsmith et al.*, 1998]. On the other hand, *Bucknam and Anderson* [1979] initiated the slope-offset analysis, allowing to estimate in a very simple manner the degradation coefficient of a one-event scarp from its maximum slope and offset. This method was improved by *Hanks and Andrews* [1989] by substituting the ''reduced scarp slope'' (maximum slope - regional slope) to the single maximum slope. Other slope-offset functions have been also derived from the diffusion equation [e.g., *Nash*, 1984]. In the case of cumulative normal fault scarps, *Avouac and Peltzer* [1993] showed that the scarp morphology, and consequently its apparent degradation state, depends on the dip of faults

that is difficult to estimate on the field without cross section of a scarp. They avoided this difficulty by comparing the reduced scarps slopes versus total offset for a significant number of scarps with those of synthetic profiles generated by a model accounting for a variable dip of faults and number of events. This process allowed the authors to bound the degradation coefficient of the studied normal fault scarp. Our results suggest that for reverse faults the fault dip is important as well for reverse faults, especially if the faulting occurs at the same location. On Figure 12, we plotted the reduced scarp slope versus cumulative offsets for different $\Delta\tau$ values and reverse fault dips in the same way as *Avouac and Peltzer*'s [1993] Figure 24b. Figure 12 shows that for a given $\Delta\tau$ value the reduced scarp slope varies according to the fault dip. The main difference with the normal faulting case studied by *Avouac and Peltzer* [1993] is that reduced scarp slopes are greater for faults dipping at 45° than for vertical faults. On one hand, decreasing fault dip in normal faulting enlarges the fault scarp and limits therefore the effect of gravitational collapse, thus decreasing the maximum slope. On the other hand, decreasing fault dip in reverse faulting leads to a scarp constriction and favors the scarp resetting by gravitational collapse, thus increasing the scarp maximum slope. In the case of low angle reverse faults, the maximum slope saturates at the slope of repose much faster than in the case of normal faulting, especially for large incremental offsets and small $\Delta\tau$ (Figure 12). Although the slope-offset method is the simplest approach, it may be limited for such scarps, providing a poor estimate of $\Delta\tau$. Moreover, because the scarp reactivation at each event does not occur always at the same location [e.g., *Avouac and Peltzer*, 1993; *Nivière and Marquis*, 2000], scarp profiles may become asymmetrical, so that the maximum slope does not provide an accurate estimate of the degradation coefficient for the whole story. This is particularly expected in the case of reverse faults and in this case, the degradation coefficient should be estimated rather from whole scarp profile.

9. Conclusions

[29] Although we did not study an exhaustive range of reverse faulting possibilities, our results suggest that an acceptable estimate of the degradation coefficient can be obtained even though basic processes such as gravitational collapse and fault dipping are neglected. In particular, the CU model is a better approximate of reverse fault than vertical fault, because the gravitational collapse balances the effect of fault dip. Moreover, we provided another solution of the diffusion equation accounting for repeated offsets and variable fault locations. Our results suggest that this model of intermediate complexity is valid for most of the cases. Our results may be used in specific studies to estimate the expected error on the calculated degradation coefficient using these two simple models and thus to evaluate the necessary level of complexity required for the dating model.

Appendix A: Derivation of the IU Model

[30] A general solution of the linear diffusion equation for elevations $h(x, \tau = K\,t)$ can be expressed as the convolution:

$$h(x,\tau) = G(x,\tau) * h(x,\tau=0)\ , \tag{A1}$$

where $h(x, \tau = 0)$ is the elevation at the location x and at an initial time. $G(x, \tau)$ is the solution for an dirac function

$$G(x,\tau) = \frac{1}{2\sqrt{\pi\,\tau}}\, e^{-\frac{x^2}{4\tau}}\ . \tag{A2}$$

For a step-like initial topography,

$$h(x,\tau=0) = 2\,a_1\,H(x) + bx\ , \tag{A3}$$

where $H(x)$ is the Heaviside function, a_1 is the half offset, and b os the regional slope. For an interseismic time $\Delta\tau_1$, the solution at $\tau = \Delta\tau_1$ is

$$h(x,\Delta\tau_1) = G(x,\Delta\tau_1) * (2\,a_1\,H(x) + bx)\ . \tag{A4}$$

If a new event occurs with a fault location at a distance Δx from the previous one, the solution at $\tau = \Delta\tau_1 + \Delta\tau_2$ can be expressed by

$$\begin{aligned} h(x,\Delta\tau_1+\Delta\tau_2) = {} & G(x,\Delta\tau_2) * \big[G(x,\Delta\tau_1) * (2\,a_1\,H(x) + bx) \\ & + 2\,a_2\,H(x+\Delta x)\big] \end{aligned} \tag{A5}$$

or

$$\begin{aligned} h(x,\Delta\tau_1+\Delta\tau_2) = {} & G(x,\Delta\tau_2) * \big[G(x,\Delta\tau_1) * (2\,a_1\,H(x) + bx)\big] \\ & + G(x+\Delta x,\Delta\tau_2) * [2\,a_2\,H(x)]\ . \end{aligned} \tag{A6}$$

Taking the derivative in space of this last expression, we can express the slope for two events in the case of a stepping fault given by

$$\begin{aligned} \frac{\partial h}{\partial x}(x,\Delta\tau_1+\Delta\tau_2) = {} & G(x,\Delta\tau_2) * G(x,\Delta\tau_1) * (2\,a_1 + b) \\ & + G(x+\Delta x,\Delta\tau_2) * 2\,a_2 \end{aligned} \tag{A7}$$

or

$$\begin{aligned} \frac{\partial h}{\partial x}(x,\Delta\tau_1+\Delta\tau_2) = {} & G(x,\Delta\tau_2+\Delta\tau_1) * (2\,a_1 + b) \\ & + G(x+\Delta x,\Delta\tau_2) * 2\,a_2\ . \end{aligned} \tag{A8}$$

Consider now the half offset a_i, the distance between fault Δx_i and the interval $\Delta\tau_i$ between events i and $i + 1$. Repeating the previous procedure for N events, the solution for slope at the event N is

$$\begin{aligned} \frac{\partial h}{\partial x}\left(x, Kt = \sum_{i=1}^{N}\Delta\tau_i\right) = {} & \sum_{i=1}^{N} \frac{a_i}{\sqrt{\pi\,\sum_{k=i}^{N}\Delta\tau_k}} \\ & \cdot \exp\left[-\frac{\left(x+\sum_{k=1}^{i}\Delta x_k\right)^2}{4\,\sum_{k=i}^{N}\Delta\tau_k}\right] + b \end{aligned} \tag{A9}$$

with $\Delta x_1 = 0$.

[31] Integrating equation (A9) in space between $-x$ and x leads to the analytical solution for elevations

$$h_{\mathrm{IU}}\left(x, Kt = \sum_{i=1}^{N} \Delta\tau_i\right) = \sum_{i=1}^{N} a_i + \sum_{i=1}^{N} a_i \,\mathrm{erf}\left[\frac{x + \sum_{k=1}^{i} \Delta x_k}{2\sqrt{\sum_{k=i}^{N} \Delta\tau_k}}\right] + x\,b \tag{A10}$$

with $\Delta x_1 = 0$.

[32] This is a solution for a vertical stepping fault with no gravitational collapse. The solution for backward step can be deduced from this expression by replacing Δxf by $-\Delta xf$.

[33] **Acknowledgments.** We thank J.-P. Avouac and an anonymous reviewer whose reviews improved greatly this paper. We are grateful to J. Verdun for numerical discussions.

References

Andrews, D. J., and T. C. Hanks, Scarp degraded by linear diffusion: Inverse solution for age, *J. Geophys. Res.*, *90*, 10,193–10,208, 1985.

Arrowsmith, J. R., D. D. Pollard, and D. D. Rhodes, Hillslope development in areas of active tectonics, *J. Geophys. Res.*, *101*, 6255–6275, 1996.

Arrowsmith, J. R., D. D. Rhodes, and D. D. Pollard, Morphologic dating of scarps formed by repeated slip events along the San Andreas Fault, Carrizo Plain, California, *J. Geophys. Res.*, *103*, 10,141–10,160, 1998.

Avouac, J.-P., Application des méthodes de morphologie quantitative à la néotectonique: Modèle cinématique des déformations actives en Asie centrale, Ph.D. thesis, Univ. Paris VII, Paris, 1991.

Avouac, J.-P., Analysis of scarp profiles: Evaluation of errors in morphologic dating, *J. Geophys. Res.*, *98*, 6745–6754, 1993.

Avouac, J.-P., and G. Peltzer, Active tectonics in southern Xinjian, China: Analysis of terrace riser and normal fault scarp degradation along the Hotan-Qira fault system, *J. Geophys. Res.*, *98*, 21,773–21,807, 1993.

Bucknam, R. C., and R. E. Anderson, Estimation of fault-scarp ages from a scarp-height-slope-angle relationship, *Geology*, *7*, 11–14, 1979.

Culling, W., Analytical theory of erosion, *J. Geol.*, *68*, 336–344, 1960.

Enzel, Y., R. Amit, N. Porat, E. Zilberman, and B. J. Harrison, Estimating the ages of fault scarps in the Arava, Israel, *Tectonophysics*, *253*, 305–317, 1996.

Hanks, T. C., The age of scarplike landforms from diffusion-equation analysis, in *Quaternary Geochronology: Methods and Applications*, *AGU Ref. Shelf Ser.*, vol. 4, edited by J. S. Noller, J. M. Sowers, and W. R. Lettis, pp. 313–338, American Geophysical Union, Washington, D.C., 1999.

Hanks, T. C., and D. J. Andrews, Effect of far-field slope on morphologic dating of scarplike landforms, *J. Geophys. Res.*, *94*, 565–573, 1989.

Hanks, T. C., and D. P. Schwartz, Morphological dating of the pre-1983 fault scarp on the Lost River fault at Doublespring Pass Road, Custer County, Idaho, *Bull. Seismol. Soc. Am.*, *77*, 837–846, 1987.

Hanks, T. C., and R. E. Wallace, Morphological analysis of the Lake Lahontan shoreline and beachfront fault scarps, Pershing County, Nevada, *Bull. Seismol. Soc. Am.*, *75*, 835–846, 1985.

Hanks, T. C., R. C. Bucknam, K. R. Lajoie, and R. E. Wallace, Modification of wave-cut and faulting-controlled landforms, *J. Geophys. Res.*, *89*, 5771–5790, 1984.

Machette, M. N., Documentation of Benchmark photograph that show the effects of the 1983 Borah Peak earthquake with some considerations for studies of scarp degradation, *Bull. Seismol. Soc. Am.*, *77*, 771–783, 1987.

Mattson, A., and R. L. Bruhn, Fault slip rates and initiation age based on diffusion equation modeling: Wasatch Fault Zone and eastern Great Basin, *J. Geophys. Res.*, *106*(B7), 13,739–13,750, 2001.

McCalpin, P., (Ed.), *Paleoseismology*, Academic, San Diego, Calif., 1996.

Meghraoui, M., H. Philip, F. Albarède, and A. Cisternas, Trench investigations through the trace of the 1980 El Asnam thrust Fault: Evidence for Paleoseismicity, *Bull. Seismol. Soc. Am.*, *78*, 979–999, 1988.

Nash, D. B., Morphological dating of fluvial terrace scarps and fault scarp near West Yellowstone, Montana, *Geol. Soc. Am. Bull.*, *95*, 1413–1424, 1984.

Nivière, B., and G. Marquis, Evolution of terrave risers along the upper Rhine Graben inferred from morphologic dating methods: Evidence of climatic and tectonic forcing, *Geophys J Int.*, *141*, 577–594, 2000.

Nivière, B., G. Marquis, and J.-C. Maurin, Morphologic dating of slowly evolving scarp using a diffusive analogue, *Geophys. Res. Lett.*, *25*, 2325–2328, 1998.

Philip, H., and M. Meghraoui, Structural analysis and interpretation of the surface deformations of the El Asnam earthquake of October 10, 1980, *Tectonics*, *2*, 17–49, 1983.

Philip, H., E. Rogozhin, A. Cisternas, J.-C. Bousquet, B. Borisov, and A. Karakhanian, The Armenian earthquake of 1988 December 7: Faulting and folding, neotectonics and paleoseismicity, *Geophys. J. Int.*, *110*, 141–158, 1992.

Swan, F. H., Temporal clustering of paleoseimsic events on the oued fodda fault, algeria, *Geology*, *16*, 1092–1095, 1988.

Wallace, R. E., Profiles and ages of young fault scarps, north-central Nevada, *Geol. Soc. Am. Bull.*, *88*, 1267–1281, 1977.

Yeatsm, R. S., K. Sieh, and C. R. Allen, *The Geology of Earthquakes*, Oxford Univ. Press, New York, 1997.

S. Carretier, BRGM, dtp ARN/MAS, 3 av. Claude Guillemin, F-45050 Orleans, Cedex 2, France. (s.carretier@brgm.fr)

F. Lucazeau, H. Philip, and J.-F. Ritz, Laboratoire de Géophysique Tectonique et Sédimentologie, UMR5573, Université Montpellier II, 4, Place Eugène Bataillon, F-34000 Montpellier, France. (francis@dstu.univ-montp2.fr; Philip@dstu.univ-montp2.fr; ritz@dstu.univ-montp2.fr)